A flexible temporal velocity model for fast contaminant transport simulations in porous media☆

Amir H. Delgoshaie[a], Peter W. Glynn[b], Patrick Jenny[c], Hamdi A. Tchelepi[a,*]

[a] *Department of Energy Resources Engineering, Stanford University. 367 Panama Street, Stanford, CA, 94305, USA*
[b] *Department of Management Science and Engineering, Stanford University. 475 Via Ortega, Stanford, CA, 94305, USA*
[c] *Institute of Fluid Dynamics, ETH Zürich. Sonneggstrasse 3, CH-8092 Zürich, Switzerland*

Abstract

In subsurface aquifers, dispersion of contaminants is highly affected by the heterogeneity of the hydraulic conductivity field. As an alternative to Monte Carlo (MC) simulations on probable conductivity fields, stochastic velocity processes have been introduced to assess the uncertainty in the transport of contaminants. In continuum scale simulations, discrete velocity models (such as correlated-CTRW) focus on modeling plume dispersion in the longitudinal direction. There are alternative continuous velocity processes (such as the polar Markovian velocity process (PMVP)) that are able to accurately model transport in both longitudinal and transverse directions. Importantly, the PMVP model correctly predicts the limited spreading of the ensemble contaminant plume in the transverse direction. However, the stochastic differential equations used in the PMVP model have specific drift and diffusion functions that are designed for the exponential correlation structure. In this paper, a new discrete velocity process is described that is applicable to modeling transport in two-dimensional conductivity fields for both Gaussian and exponential correlation structures. This method is simple, in a sense that it does not require modeling the functional form of the drift and diffusion functions. The new method is validated against Monte Carlo (MC) simulations for both correlation structures with high variances of log-conductivity.

Keywords: anomalous transport, Markov models, stochastic transport modeling, stencil method

1. Introduction

Modeling transport in porous media is highly important in various applications including water resources management and extraction of fossil fuels. Predicting flow and transport in aquifers and reservoirs plays an important role in managing these resources. Two significant factors influencing transport are the heterogeneity and the uncertainty of the underlying conductivity field. The classical strategy to deal with these two factors is to perform Monte Carlo (MC) simulations on probable conductivity fields which can have a very high computationally cost. Moreover, ensemble statistics of transport in heterogeneous domains displays non-Fickian characteristics such as long tails for the first arrival time probability density function (PDF) and non-Gaussian spatial distributions [1, 2, 3]. Capturing this non-Fickian behavior is particularly important for predictions of contaminant transport in water resources. For example, in water resources management long tails of the arrival time PDF can have a major impact on the contamination of drinking water, and therefore efficient predictions of the spatial extents of contaminant plumes is key [4, 5, 6].

Past studies have provided a range of Lagrangian models for efficient prediction of this non-Fickian transport. The continuous time random walk (CTRW) formalism offers a framework to study anomalous transport through disordered media and networks [1, 7]. The time domain random walk method (TDRW), which is conceptually similar to the CTRW method, directly calculates the arrival time of a particle cloud at a given location [8, 9]. Similar to CTRW, consecutive velocities resulting from the TDRW method are independent of each other. Detailed studies of transport have shown conclusively that for long times/distances, particle velocities in mass conservative flow fields are correlated [10, 11] and accounting for this correlation is crucial, specifically in cases with a high variances of the log-conductivity field. To account for this correlation, Markov velocity models have been developed. The proposed Markov models can be classified based on the underlying medium that they model (network vs. continua), the variables chosen to index the stochastic velocity process (temporal, spatial, and mixed (temporal and spatial) models), and finally based on whether the models are discrete or continuous (discrete Markov chains

☆This article has been published in WRR: Delgoshaie, A. H., Glynn, P. W., Jenny, P., & Tchelepi, H. A. (2018). A flexible temporal velocity model for fast contaminant transport simulations in porous media. Water Resources Research.

*Corresponding author
Email address: tchelepi@stanford.edu (Hamdi A. Tchelepi)

vs. stochastic differential equations). In the next two paragraphs, a short summary of some of the relevant correlated velocity models is provided. In the view of the suggested classification, the model proposed here is a discrete temporal model for continuum scale problems.

Le Borgne et al. [12] proposed discrete Markov chains for modeling the velocity process and tested the Markov assumption for the longitudinal component of the velocity of tracer particles in heterogeneous porous media. They studied transition probabilities for the velocity process in time and space. Subsequently, A one-dimensional spatial Markov model was used in [13] to successfully model transport in correlated heterogeneous domains. Kang et al. [14, 15, 16] extended the discrete spatial Markov model framework to two dimensions and performed several studies on random lattice networks. Similar structured and unstructured random lattice networks were simulated with discrete temporal velocity models (the stencil method) in [17]. The spatial Markov model was also applied to the velocity field resulting from simulation of flow in the pore space of real rock and to disordered fracture networks [18, 19].

Meyer et al. used a temporal Markov model and successfully modeled particle dispersion in two-dimensional correlated conductivity fields using stochastic differential equations [20]. This framework was then used to model the joint velocity-concentration PDF [21]. In another study, Meyer and Saggini [22] provided a framework for testing the Markov hypothesis for the velocity of tracer particles. In the class of mixed temporal and spatial models, Meyer et al. [23] proposed the polar Markov velocity process (PMVP). The PMVP model consists of a set of SDEs for modeling transport in exponential permeability fields with a velocity process in time and an angle process in space. Another mixed set of SDEs were proposed to model the velocity process resulting from direct numerical simulation (DNS) of flow and transport in the pore-space of real rocks [24].

For modeling transport in correlated continuum scale permeability fields, two-dimensional simulations are often performed for uncertainty quantification. In two-dimensions, the ensemble contaminant plume has the interesting property that it asymptotically stops spreading in the transverse direction [25]. Among the stochastic models proposed for modeling ensemble transport in continuous correlated conductivity fields, some studies focus on transport in the longitudinal direction and propose a one-dimensional model that accurately captures the transport characteristics in the longitudinal direction [13]. In the literature, to the extent of the authors' knowledge, the limited spreading of the plume in the transverse direction was only captured by the stochastic differential equations proposed in [20, 23].

In both [20] and [23] the proposed SDEs have specific drift and diffusion functions that are designed for the specific study. For example, the PMVP model proposed in [23] consists of an SDE in space for the velocity angle process and an independent SDE in time for the velocity magnitude process. These SDEs have specific drift and diffusion terms that work for conductivity fields with exponential correlation structure with log-conductivity variances between 1/16 and 4. These drift and diffusion functions vary for different studies (compare [20] and [24]). For modeling transport in correlated continuum scale problems, the available SDE models are designed for an exponential correlation structure, and a PMVP model for a Gaussian conductivity correlation structure is not available. Moreover, educated insight is required for designing appropriate drift and diffusion function for new scenarios.

In this work, we use a discrete temporal Markov velocity process (referred to as DTMVP). Compared to the PMVP model, the model proposed here does not require modeling the functional form of the drift and diffusion terms. Hence, it is applicable to both exponential and Gaussian correlation structures. Compared to other previously proposed one-dimensional discrete models for continua (e.g. [12, 13]), the DTMVP model can make accurate predictions in both transverse and longitudinal directions. Similar to PMVP, DTMVP also correctly predicts the limited spreading of the ensemble contaminant plume in the transverse direction. In the next two sections, the transport problem and particle tracking setup are explained in detail. The DTMVP model is described in section 4. The results are discussed in section 5 and DTMVP is compared to the stencil method in section 6. Conclusions are given in section 7.

2. The single-phase transport problem

We study single-phase flow and transport in porous media. The velocity field of the fluid is calculated by Darcy' s law

$$\mathbf{u}(\mathbf{x}) = -\mathbf{K}(\mathbf{x})\nabla h(\mathbf{x}), \tag{1}$$

where $\mathbf{K}(\mathbf{x})$ is the hydraulic conductivity field. We study incompressible flow, where the hydraulic head, $h(\mathbf{x})$, can be found by solving the continuity equation $\nabla.\mathbf{u} = 0$, leading to

$$\nabla.(\mathbf{K}(x)\nabla h(\mathbf{x})) = 0. \tag{2}$$

Once the hydraulic head and the velocity field are known, assuming negligible pore-scale dispersion (PSD) and diffusion, the transport of a contaminant is governed by the advection equation

$$\frac{\partial C}{\partial t} + \frac{\partial}{\partial x_i}(u_i C) = 0, \tag{3}$$

where $C(\mathbf{x}, t)$ is the tracer concentration at position $\mathbf{x}$ and time t, and u_i is the ith component of the velocity vector $\mathbf{u}$. Tracking Lagrangian tracer particles is an alternative to solving the advection equation for the tracer concentration. The particle tracking problem setup is elaborated in the next section.

3. Particle tracking problem setup

We consider log-normal permeability distributions with variances up to four. The particle tracking setup is chosen very similar to [20, 13]. Meyer et al. studied a case with an exponential correlation function, whereas Le Borgne et al. studied a Gaussian correlation structure. Here we consider both correlation structures. For both correlation structures the correlation length (l_Y) is chosen equal to 8 grid cells. The computational domain is a square with each edge length L equal to $128 l_Y$ (1024 cells). In this study all four boundaries for the generated conductivity fields are periodic, in the sense that the correlation structure is preserved across all boundaries. Figure 1 illustrates the periodicity of the generated conductivity fields. These periodic conductivity fields are generated using the Fourier integral method described in [26]. The flow equation is also solved using periodic boundary conditions. This periodic setup allows us to generate longer particle trajectories by allowing particles to pass multiple times through the domain. Due to the periodicity of the domain boundary effects are not present in the particle trajectories generated in this study.

In the considered problem, the mean velocity in the longitudinal direction is U and the mean transverse velocity is zero. For each correlation structure and each log-conductivity variance, 500 realizations were generated. In each realization a periodic flow problem was solved. The flow problem was solved using a finite-volume discretization and the resulting linear systems were solved using an efficient algebraic multigrid solver [27].

In each realization 108 tracer particles were tracked through the conductivity field. Each particle is tracked until it travels 2400 times between cells. In order to fully sample the velocity field in each realization, tracer release locations were separated by l_Y. All particles were released on the left boundary with a minimum distance of $10 l_Y$ to the top and bottom boundaries. Fig. 2 illustrates this periodic particle tracking setup. The Integration of velocity along a particle trajectory was performed using the algorithm described in [28].

4. Describing the model

The model proposed in this work consists of two independent processes for the particle velocity magnitude and the particle velocity angle. It has been previously shown that independence of the two processes in polar coordinates can be approximately validated, even for cases with high variance of log-conductivity [23]. In this section both processes are described in detail. Both velocity and angle processes are in time, which means that we model the temporal evolution of the particle velocity vector at times $t_0 = 0, \Delta t_s, 2\Delta t_s$, etc. Here, Δt_s is the averaging time step which is a model input parameter. In has been shown in previous studies that the velocity process can be far from Markovian for relatively small values of Δt_s [22]. Figure 3 shows a sample particle trajectory and the same trajectory averaged with different values of Δt_s. The averaging time steps is described in terms of the characteristic time scale of the problem $\overline{\delta t} = l_Y/U$. Next, both the velocity and angle process are described in detail. In the remainder of the manuscript the velocity and angle distributions that are used for inferring model parameters are empirical distributions generated by analyzing particles trajectories from the MC simulations.

4.1. The velocity magnitude process

The velocity magnitude process (also referred to as the velocity process) used here is a discrete Markov chain for the average velocity in time. The average velocity is divided into discrete classes as follows:

$$v \in \cup_{j=1}^{n_v} (log(\overline{v})_j, log(\overline{v})_{j+1}), \tag{4}$$

where n_v is the number of velocity magnitude classes. As previously suggested in [20], in order to better represent slow transitions we use the logarithm of velocity magnitude for the definition of classes. The velocity magnitude bin edges are first chosen such that the bins have equal probability. Since there are not many extremely slow or extremely fast particles, the bins corresponding to these classes would be comparatively large. The extreme velocity bins are further refined to have the final velocity magnitude bins. The velocity bin corresponding to the smallest velocity magnitudes is split into 10 smaller bins and the 10 bins corresponding to the fastest velocities are adjusted such that their width is smaller than a specified threshold. For details of the refinement procedure, please refer to the provided repository [29].

We refer to the discrete transition matrix for the velocity magnitude as $p_m^v(i|j)$. This is the probability of encountering the state i after m transitions, assuming that we started from the state j. The one-step velocity transition matrix $p_1^v(i|j)$ for the exponential correlation structure for $\Delta t_s = 10\overline{\delta t}$ is illustrated in Fig. 4.

It has been previously shown in [22] that a Markovian process is a good approximation for the velocity process for $\Delta t_s > 2.56\overline{\delta t}$. Provided that a Markov process can closely model transitions between different velocity states, we expect that the Chapman-Kolmogorov (CK) relation holds for these transitions. We perform a test to compare

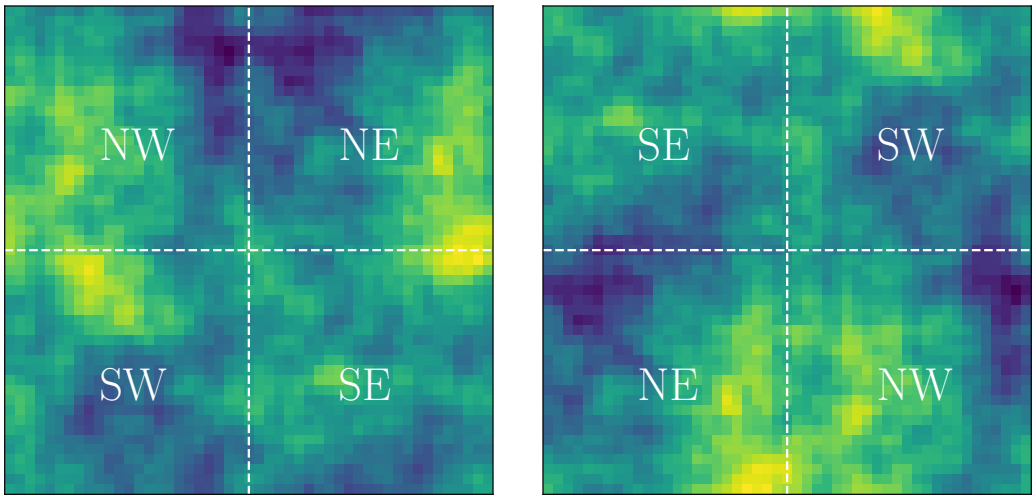

Figure 1: Illustration of the periodicity of the generated conductivity fields. Shuffling the four quarters of a generated permeability field leads to a new field which has the same correlation structure.

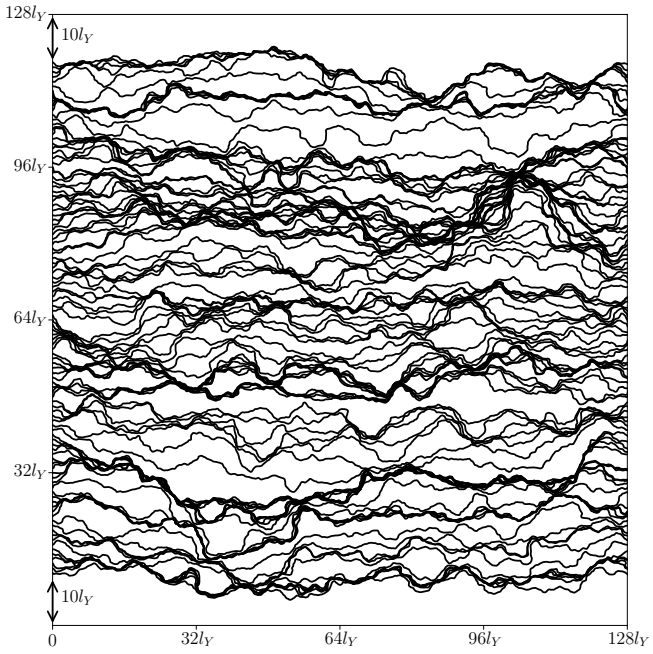

Figure 2: Trajectories in one realization of the conductivity field with the Monte Carlo particle tracking setup described in section 3.

the m-step velocity transition with the m-fold product of the one-step transition matrices. The five-step velocity transition matrix $p_5^v(i,j)$ is compared to $p_1^v(i,j)^5$ in Fig. 5 for $\Delta t_s = 10\overline{\delta t}$. Column-wise comparison of these two matrices is illustrated in Fig. 6 for transitions from a fast and a slow initial velocity class.

Similar comparisons were performed for the Gaussian correlation structure (see supporting information). The results suggest that a Markov model is a good candidate to accurately represent the velocity process for both correlation structures considered in this study.

4.2. The angle process

Here our goal is to explore the possibility of using discrete temporal models for modeling transport in highly heterogeneous correlated permeability fields. An important feature of the two-dimensional problem studied here

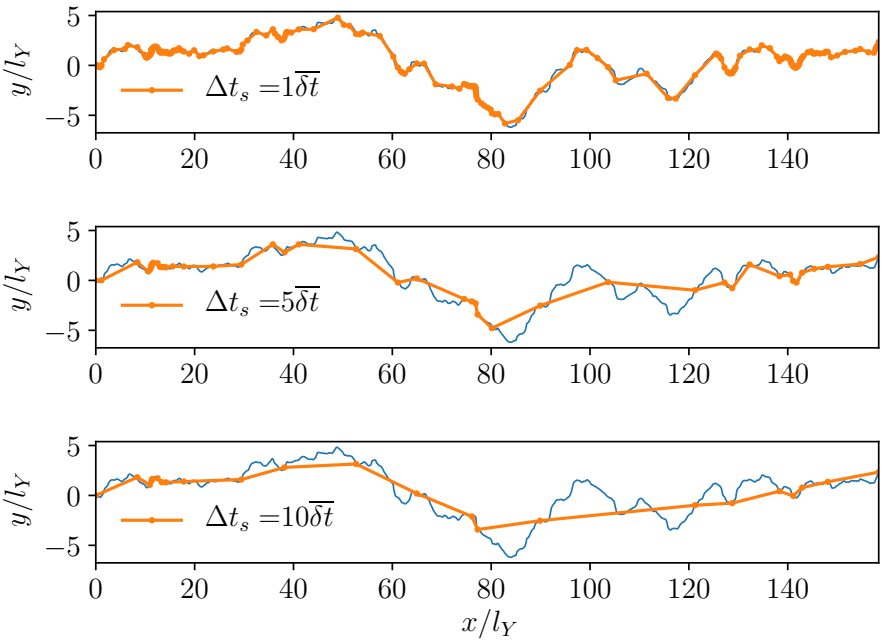

Figure 3: A particle trajectory and the average representation of the same trajectory with three different time steps.

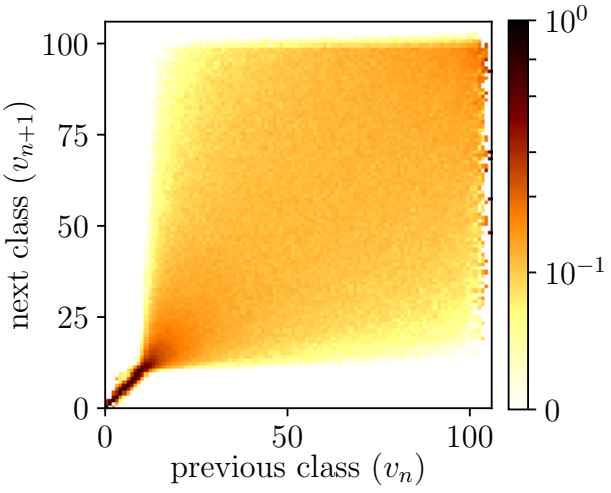

Figure 4: $p_1^v(i|j)$ for the exponential correlation structure for $\Delta t_s = 10\overline{\delta t}$. Square root of the transition matrix is plotted for better contrast.

is the limited spreading of the plume in the transverse direction [25]. Heuristically, this means that particles that travel laterally too far from their injection point would, on average, travel back towards that point. The distribution of the particle angle conditional on the normalized distance from injection, $p(\theta|\overline{y})$, confirms this heuristic. The left portion of fig. 7, shows $p(\theta|\overline{y})$ for the exponential correlation structure for $\Delta t_s = 10\overline{\delta t}$. To build the discrete distribution of $p(\theta|\overline{y})$, the interval $[-\pi, \pi]$ was divided into n_θ bins. Here

$$\theta \in \cup_{j=1}^{n_\theta}(\overline{\theta}_j, \overline{\theta}_{j+1}) \tag{5}$$

represents the state of the velocity angle. Similarly the normalized distance from injection is discretized in to n_y bins. The left portion of Fig. 7 shows the result of filling this histogram by counting the observed angles at each value of $\overline{y}$. In order to use this distribution for simulating contaminant plumes, one would need to approximate the distribution for values of $\overline{y}$ where the histogram is noisy. In other words it is necessary to "fill the holes in data". Fortunately, there are clear observable trends in this distribution. These trends can be used to extrapolate the distribution from values of $\overline{y}$ were the distribution is well captured by the histogram to larger values of $|\overline{y}|$ where the distribution is noisy.

The procedure used for filling the holes in the conditional angle distribution is as follows. First, we fit a known PDF template, Pearson type 3 (Pearson3), to $P(\theta|\overline{y})$ for a set of y values where the histogram is not noisy. Then the first three moments of the fitted distributions are approximated as constants or linear

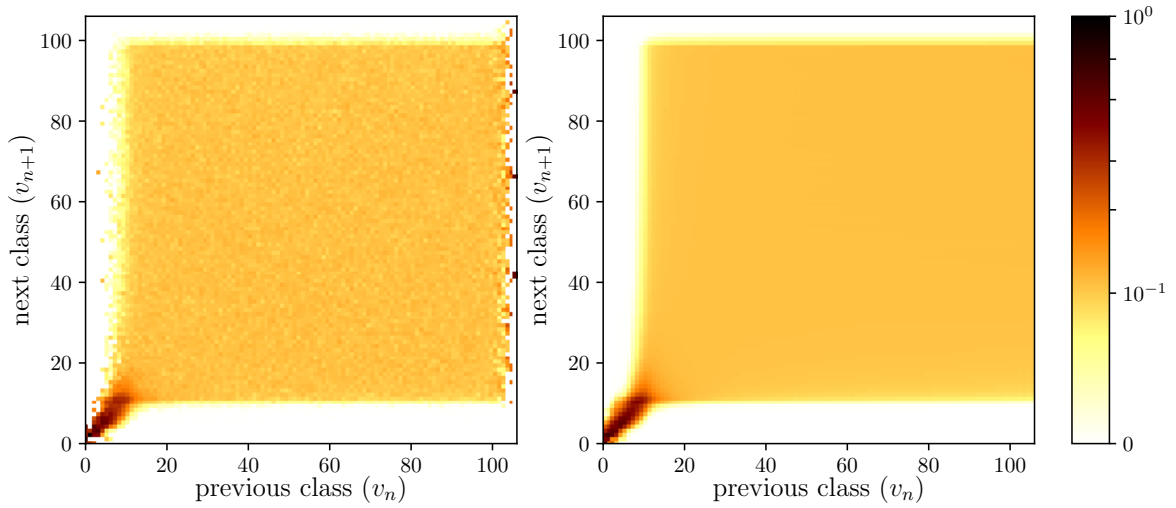

Figure 5: Comparison of $p_5^v(i,j)$ (left) and $p_1^v(i,j)^5$ (right) for the exponential correlation structure for $\Delta t_s = 10\overline{\delta t}$. Square root of the transition matrices are plotted for better contrast.

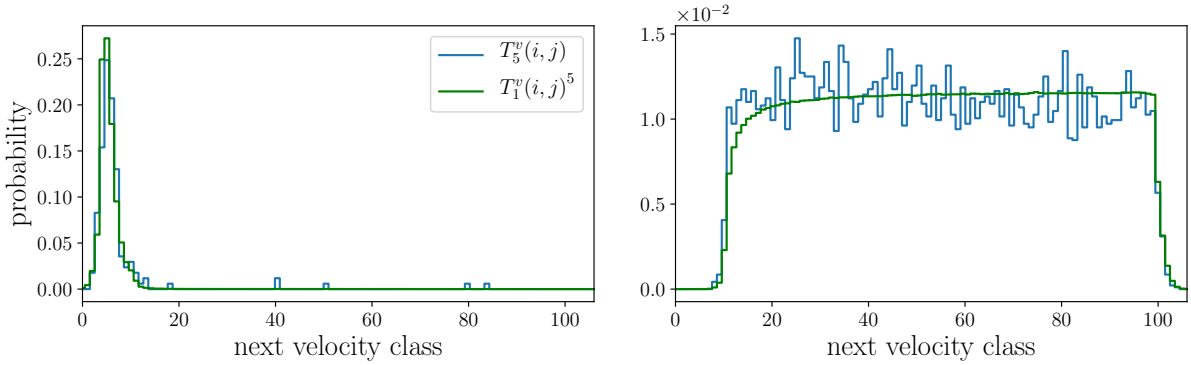

Figure 6: Column-wise comparison of $p_5^v(i,j)$ and $p_1^v(i,j)^5$ for the exponential correlation structure for $\Delta t_s = 10\overline{\delta t}$. Left: initial class $j = 4$; right: initial class $j = 62$.

functions of $\overline{y}$. Specifically, a linear relation was used for the first and third moments and the variance was approximated by a constant. These moments are then extrapolated to the values of y where the distribution is noisy. Finally, the noisy distributions are approximated by using the known form of the Pearson3 PDF and its first three moments. Figure 8 shows the result of fitting a Pearson3 PDF to $P(\theta|\overline{y})$ for two different values of $\overline{y}$. The first three moments of the fitted distribution and the low order fits to these moments are shown in Fig. 9. As the final result of this procedure, Fig. 7 shows the comparison between the histogram obtained from the MC data and the model histogram built using the moments of Pearson3 distribution.

The same procedure was applied to the MC simulation results for the Gaussian correlation structure, resulting in similar observations which are included in the supporting material. The most notable difference observed in the moments of the Gaussian correlation structure compared to the exponential correlation structure is the clear linear trend observable for the third moment of the empirical angle distribution.

4.3. Simulating the particle plume using the proposed stochastic model

Given $p_1^v(i|j)$, $p(\theta|\overline{y})$ and initial distributions for the logarithm of the velocity magnitude ($p(v_0)$) and angle ($p(\theta_0)$) a particle plume can be simulated using algorithm 1. We refer to this model as the discrete temporal Markov velocity process (DTMVP).

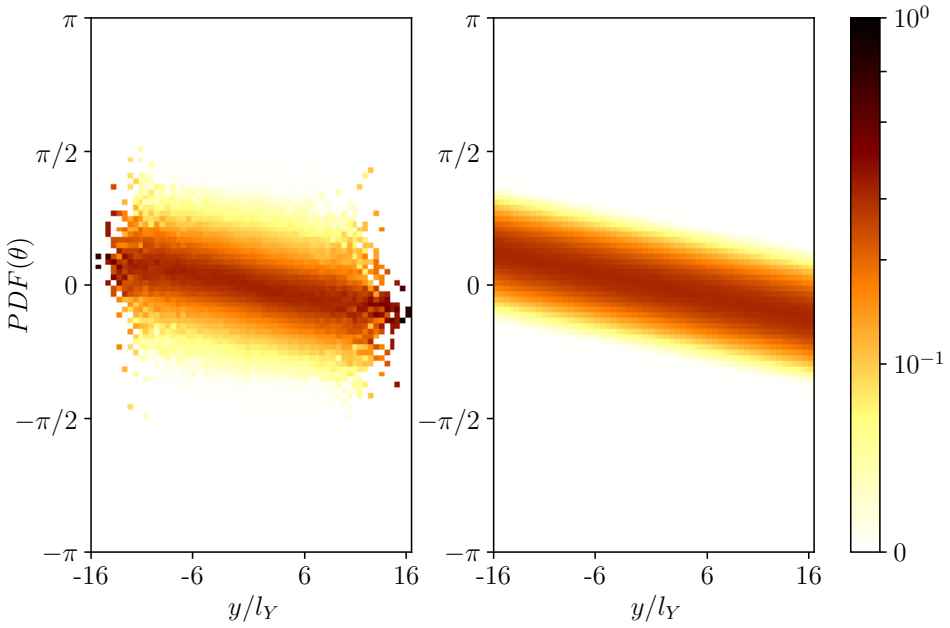

Figure 7: $P(\theta|\overline{y})$ for the exponential correlation structure with $\Delta t_s = 10\overline{\delta t}$. Left: empirical distribution from MC simulations; right: modeled histogram using the extrapolated moments of Pearson3 distribution.

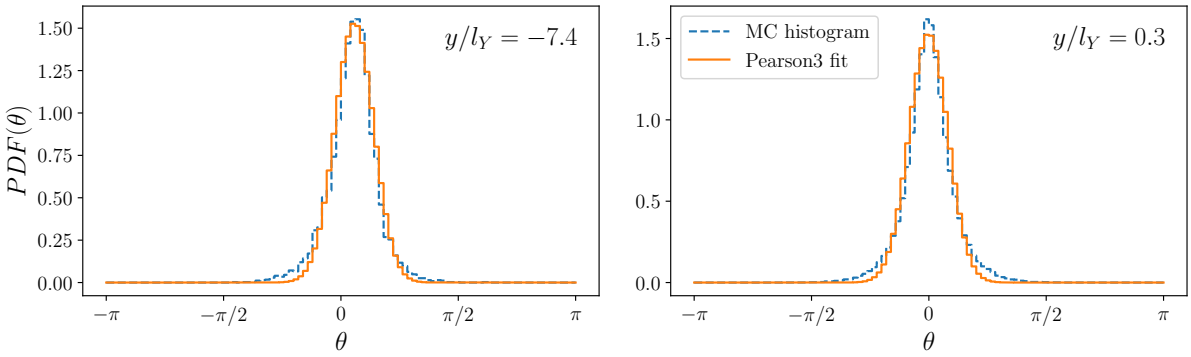

Figure 8: Comparison of $P(\theta|\overline{y})$ for two different values of $\overline{y}$ for the exponential correlation structure for $\Delta t_s = 10\overline{\delta t}$.

5. Results

The DTMVP model was applied to the MC data described in section 3 for both exponential and Gaussian correlation structures with log-permeability variances of 1, 2, 4. The results for $\sigma^2 = 1, 2$ are not included in this manuscript for brevity. The results for the highest variance case for the exponential correlation structure are presented below. Corresponding figures for the Gaussian correlation structure are included in the supporting material.

We start by describing the results for the exponential correlation structure with a variance of 4, and an averaging time step $\Delta t_s = 10\overline{\delta t}$. The results for smaller and larger time steps are also discussed in this section. The model parameters used for DTMVP are listed in table 1. The two-dimensional plumes generated by DTMVP are compared with the MC data in Figure 10. The extents of the ensemble plumes are well captured by the DTMVP model. For a closer inspection, the projection of the plume on the longitudinal and transverse directions is compared to the MC data in figures 11 and 12 for two different times. The spreading of the plume is well captured by the DTMVP model in both longitudinal and transverse directions.

In these results we are averaging the particle trajectory

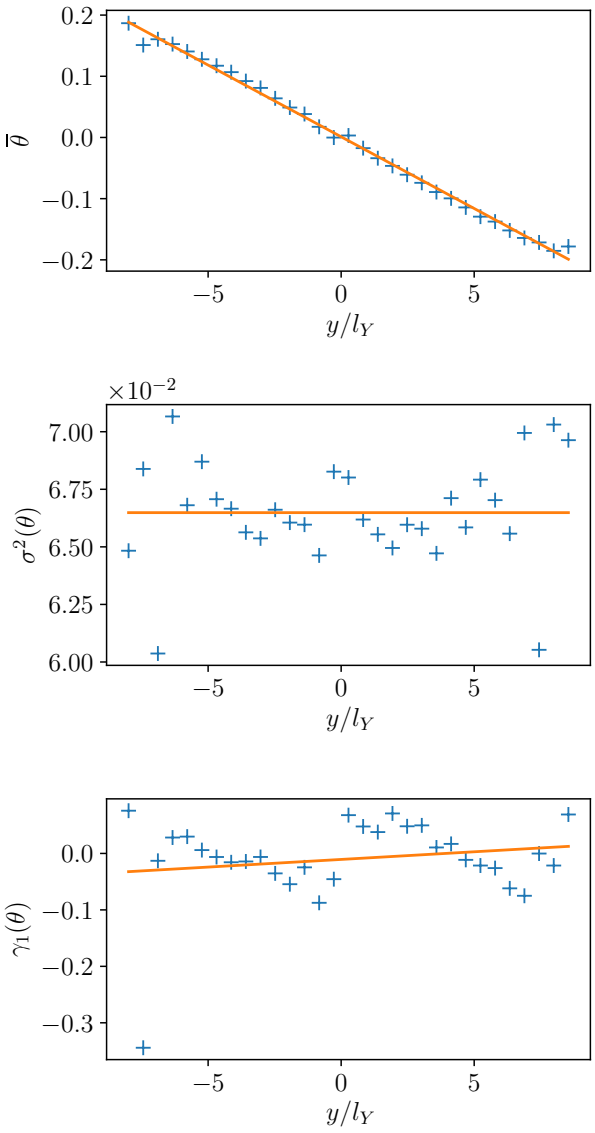

Figure 9: First three moments of $P(\theta|\overline{y})$ as a function of $\overline{y}$, for the exponential correlation structure with $\Delta t_s = 10\overline{\delta t}$.

with a time step $\Delta t_s = 10\overline{\delta t}$. As it can be seen in Fig. 3, this is a relatively course time step. With larger time steps the average velocities would become less correlated. One can argue that with very large stencil times, using a correlated random walk model would no longer be necessary and independent spatial increments would be sufficient for modeling the dispersion process at very low temporal resolutions. In order to inspect the added value by the DTMVP model compared to independent sampling from the joint (v, θ) distribution, a numerical experiment is performed. We model the particle plume according to algorithm 2 and compare the results with the DTMVP model. Figures 13 and 14 illustrate the results of this experiment for a wide range of time steps ($1\overline{\delta t} < \Delta t_s < 10\overline{\delta t}$). As

```
// initialization
v_0, θ_0 ← draw from p(v_0), p(θ_0);
x_0, y_0 ← 0, 0;
for i ← 1 to n do
    // advance the particle location given
       current velocity vector
    x_i = x_{i-1} + exp(v_{i-1}) cos(θ_{i-1}) Δt_s;
    y_i = y_{i-1} + exp(v_{i-1}) sin(θ_{i-1}) Δt_s;
    // draw next log velocity magnitude given
       current magnitude
    v_i ← draw from p_1^v(v_i | v_{i-1});
    // draw next angle given normalized
       transverse distance from injection
    θ_i ← draw from P(θ_i | ȳ_i);
end
```

Algorithm 1: Particle evolution with DTMVP

parameter	value
n_v	106
n_θ	100
n_y	60
# particles	500×108

Table 1: DTMVP simulation parameters for both Gaussian and exponential correlation structures.

these results suggest, neglecting the velocity correlations and the dependence of angle on $\overline{y}$ would lead to inaccurate estimates of the plume. On the other hand, the DTMVP model make accurate predictions for all the time steps between $\overline{\delta t}$ and $10\overline{\delta t}$. As it can be observed in Fig. 13, the slow tail of the plume is better captured using larger values of Δt_s.

Our experiments show that in comparison with the exponential correlation structure, for the Gaussian correlation structure a larger average time step is required for accurate predictions of the plume (results for the Gaussian case are included in the supporting information). This observation is consistent with previously reported results [22].

The evolution of the dimensionless mean square differences (MSD) of the plume predicted by algorithm 2, in both longitudinal and transverse directions is depicted in Fig. 15. For this plot and all subsequent dimensionless moment plots of the plumes, l_Y is used as the nondimensionalization length scale. This figure confirms that for the wide range of tested time steps, independent sampling from the joint distribution of (v, θ) is not sufficient to model the dispersion of the ensemble plume. Specifically, independent sampling leads to ensemble plumes that scale differently from the MC data in both longitudinal and transverse directions.

Compared to the MC data, the projection of the plume onto the transverse direction displays a more distinctive peak near the origin. This peak is mainly due to the fact that the model for the angle process does not include

a direct dependence on the angle history. In the next section, this idea is explored in detail by comparing the results to the results of the stencil method [17] where $p(v_{n+1}, \theta_{n+1}|v_n, \theta_n)$ is used.

// initialization
$v_0, \theta_0 \leftarrow$ draw from $p(v_0), p(\theta_0)$;
$x_0, y_0 \leftarrow 0, 0$;
for $i \leftarrow 1$ **to** n **do**
  // advance the particle location given current velocity vector
  $x_i = x_{i-1} + exp(v_{i-1})cos(\theta_{i-1})\Delta t_s$;
  $y_i = y_{i-1} + exp(v_{i-1})sin(\theta_{i-1})\Delta t_s$;
  // draw next log velocity magnitude and angle from their joint distribution
  $v_i, \theta_i \leftarrow$ draw from $p(v, \theta)$
end

Algorithm 2: Plume evolution with independent sampling from $p(v, \theta)$

6. Comparison to the stencil method

The stencil method [17] is also a discrete temporal process that models the evolution of particle velocities as a Markov chain for the (v, θ)-pair (see algorithm 3). Similar to the DTMVP model, the correlation between the magnitude of consecutive particle velocities is captured by the stencil method. Unlike the DTMVP model, the stencil method does not use any heuristic for limiting the particle velocity angle. In this section we study the effect of the restricted angle process in the DTMVP model on predicted plumes by comparing the results to the stencil method.

The stencil method was applied to the generated MC data for both Gaussian and exponential correlation structures, and the results are compared with the DTMVP model for the range of averaging time steps, $1 < \Delta t_s/\overline{\delta t} < 20$. The results show very similar trends for both correlation structures. For brevity, only the results for the exponential correlation structure with log-conductivity variance of four are presented in this section. Comparison of the projection of the predicted plumes on the longitudinal direction, illustrated in Fig. 16, shows that both models make accurate predictions for dispersion along the mean flow direction. Figures 17 and 18 show that both the stencil method and the DTMVP model make similar predictions for the evolution of the center of mass and mean square difference of the longitudinal projection of the plume.

The two models have a notable difference in predicting the BT curve. Figure 19 shows that the DTMVP models makes more accurate predictions for the first passage time curve of the vertical plane $x = 0.75L$, for $1 < \Delta t_s/\overline{\delta t} < 10$.

// initialization
$v_0, \theta_0 \leftarrow$ draw from $p(v_0), p(\theta_0)$;
$x_0, y_0 \leftarrow 0, 0$;
for $i \leftarrow 1$ **to** n **do**
  // advance the particle location given current velocity vector
  $x_i = x_{i-1} + exp(v_{i-1})cos(\theta_{i-1})\Delta t_s$;
  $y_i = y_{i-1} + exp(v_{i-1})sin(\theta_{i-1})\Delta t_s$;
  // draw next log velocity magnitude and angle from their conditional joint distribution
  $v_i, \theta_i \leftarrow$ draw from $p(v_i, \theta_i|v_{i-1}, \theta_{i-1})$
end

Algorithm 3: Plume evolution with the stencil method

For $\Delta t_s = 20\overline{\delta t}$, both models make inaccurate predictions for the BT curve. The predictions of the transverse plume for the two models are qualitatively different, as illustrated in Fig. 20. The peak in the DTMVP model predictions is not present in the stencil method results. Figure 20 also shows that the extent of the transverse plume predicted by the stencil method changes as a function of Δt_s, whereas the extent of the DTMVP model prediction does not change significantly by changing the averaging time. This is a consequence of the heuristic ($P(\theta|\overline{y})$) built into the DTMVP method.

The evolution of the dimensionless second central moment of the transverse plume is shown in Fig. 21. For $1 < \Delta t_s/\overline{\delta t} < 10$, the stencil method predicts an ensemble plume that keeps growing in the transverse direction. However, for a wide range of time steps, $4 < \Delta t_s/\overline{\delta t} < 20$, the transverse MSD predicted by DTMVP stops growing which qualitatively matches the behavior observed in the MC data and expected from [25].

7. Conclusions

In this work, DTMVP, a flexible discrete stochastic process has been proposed for modeling transport in high variance correlated conductivity fields with Gaussian and exponential correlation structures. The proposed model is the first fully temporal two-dimensional velocity process for transport in continuum scale. With respect to previously proposed one-dimensional correlated-CTRW models for transport in correlated conductivity fields, DTMVP is an alternative that can be used for making predictions in both longitudinal and transverse directions. Compared to the PMVP model, the proposed model is fully temporal and does not require modeling the functional form of the drift and diffusion terms utilized in PMVP. This simplicity, allows DTMVP to be applied to both Gaussian and exponential correlation structures without any modification. Compared to the stencil method, DTMVP makes more accurate predictions for breakthrough curves and the transverse spreading of the ensemble plume.

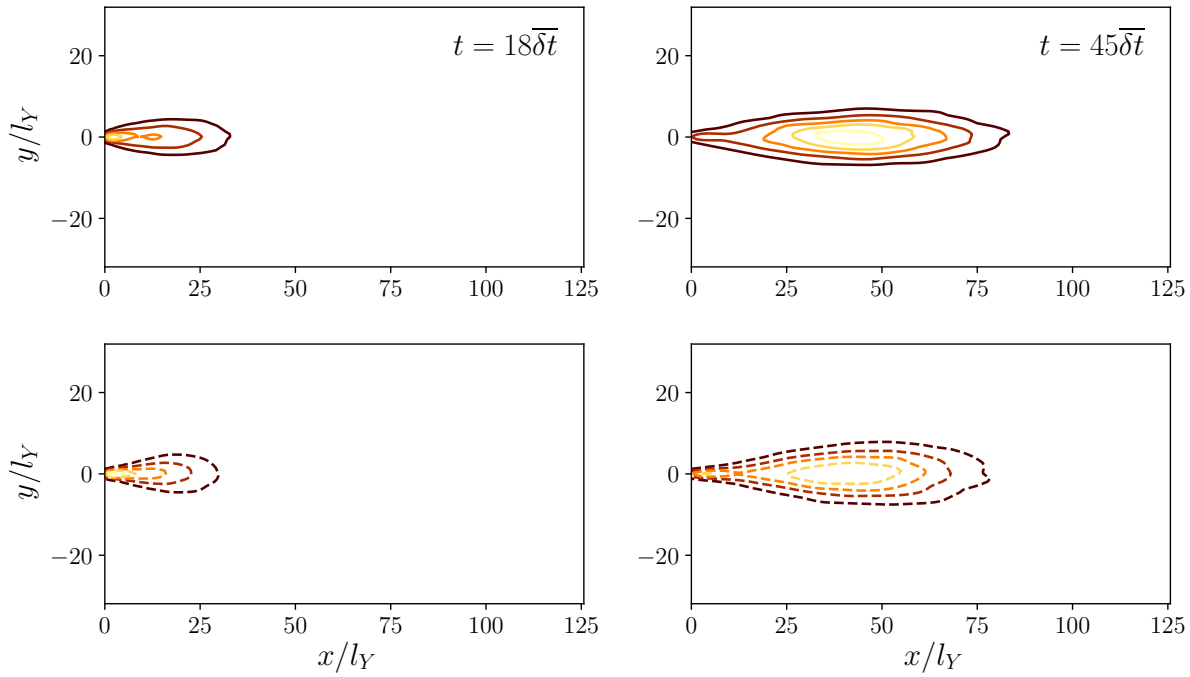

Figure 10: Comparison of the predicted plume (solid lines) versus the MC data (dashed lines) for two different times for the same contour levels for the exponential correlation structure.

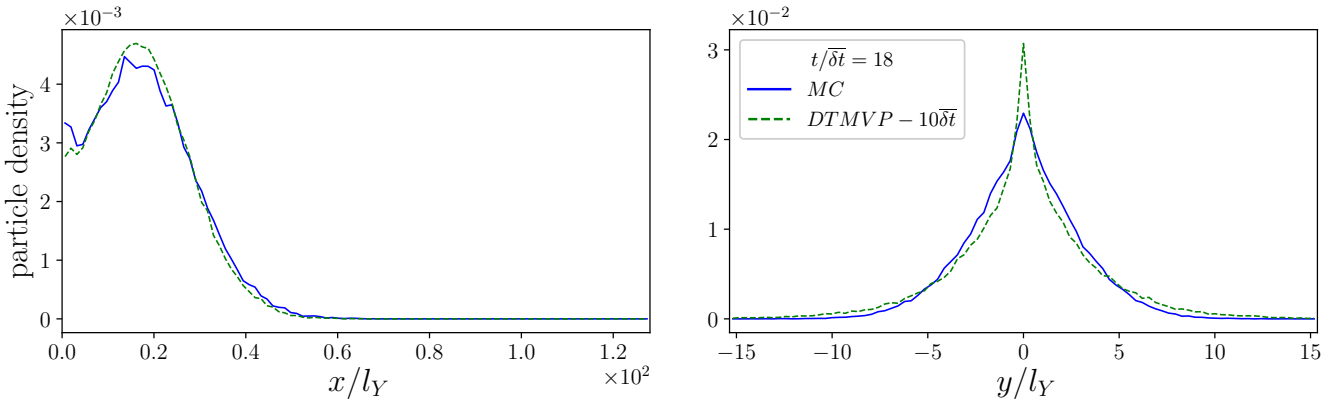

Figure 11: Comparison of the predicted plume versus the MC data for $t = 18\overline{\delta t}$ for the exponential correlation structure.

Acknowledgements

The data for generating the plots and the code used for generating the complete data set and the velocity models are available at https://github.com/amirdel/dispersion-continua. Amir H. Delgoshaie is grateful to Daniel Tartakovsky from the Energy Resources Engineering department at Stanford University for several helpful discussions. Funding for this project was provided by the Stanford University Reservoir Simulation Industrial Affiliates (SUPRI–B) program.

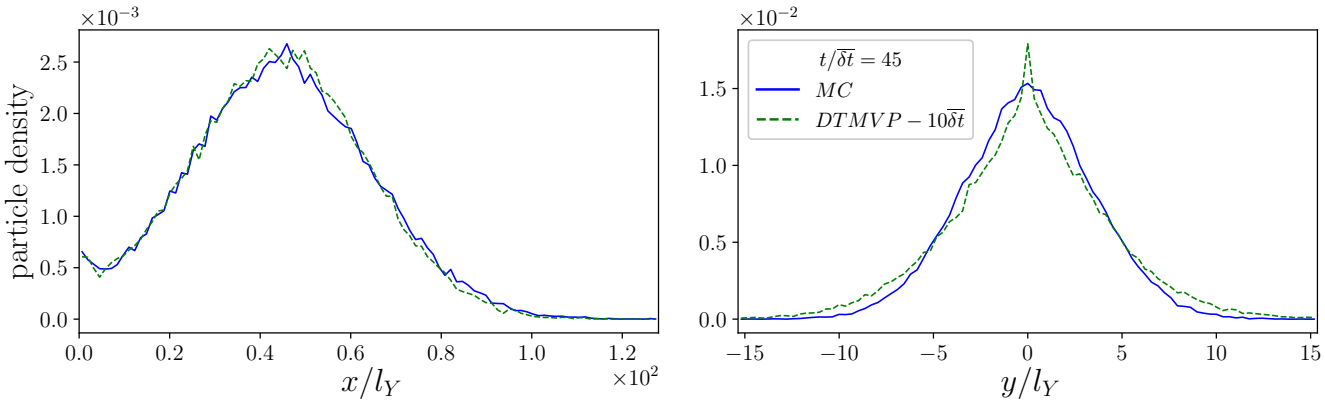

Figure 12: Comparison of the predicted plume versus the MC data for $t = 45\overline{\delta t}$ for the exponential correlation structure.

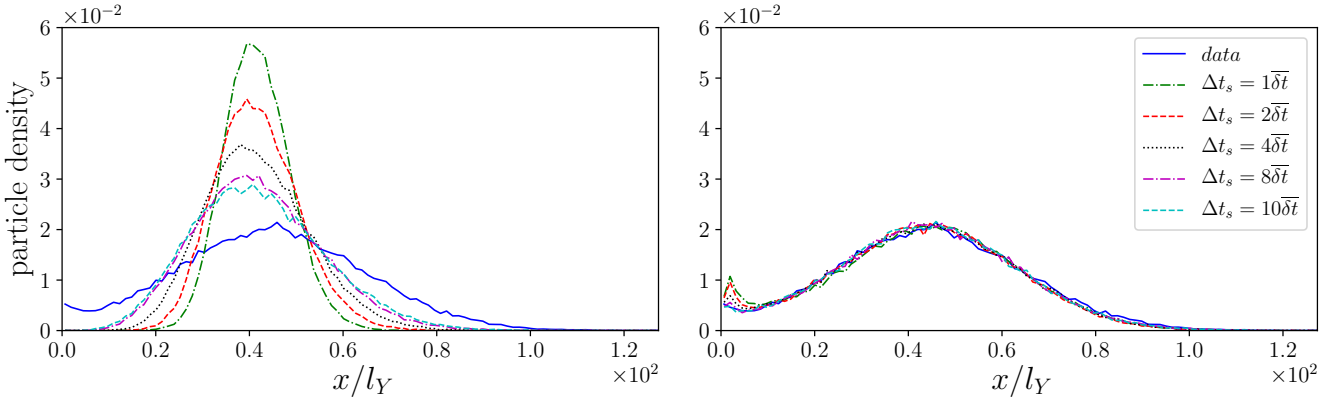

Figure 13: Comparison of the predicted plumes from the independent model (left) and DTMVP (right) at $t = 45\overline{\delta t}$ for different time steps for the exponential correlation structure.

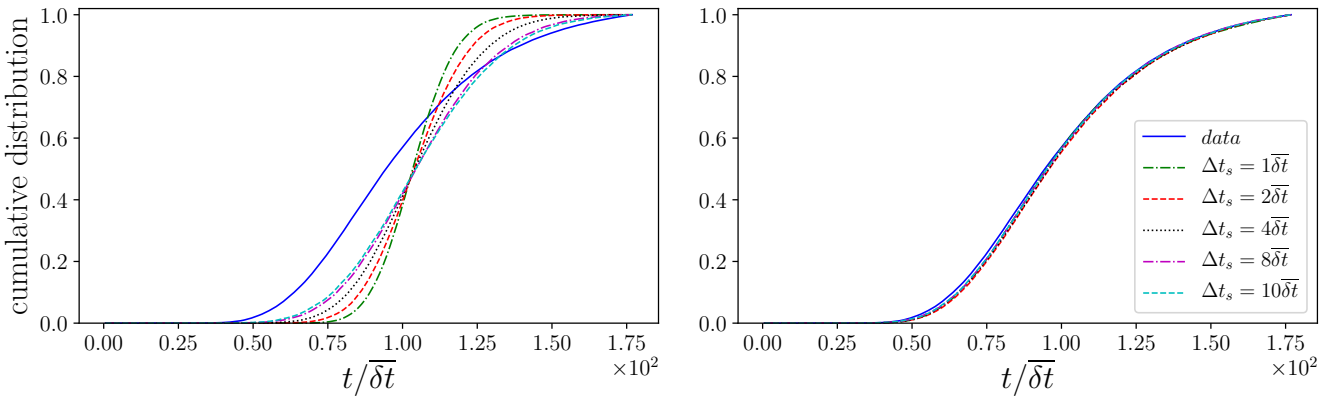

Figure 14: Comparison of the predicted BT curves from the independent model (left) and DTMVP (right) at $x = 0.75L$ for different time steps for the exponential correlation structure.

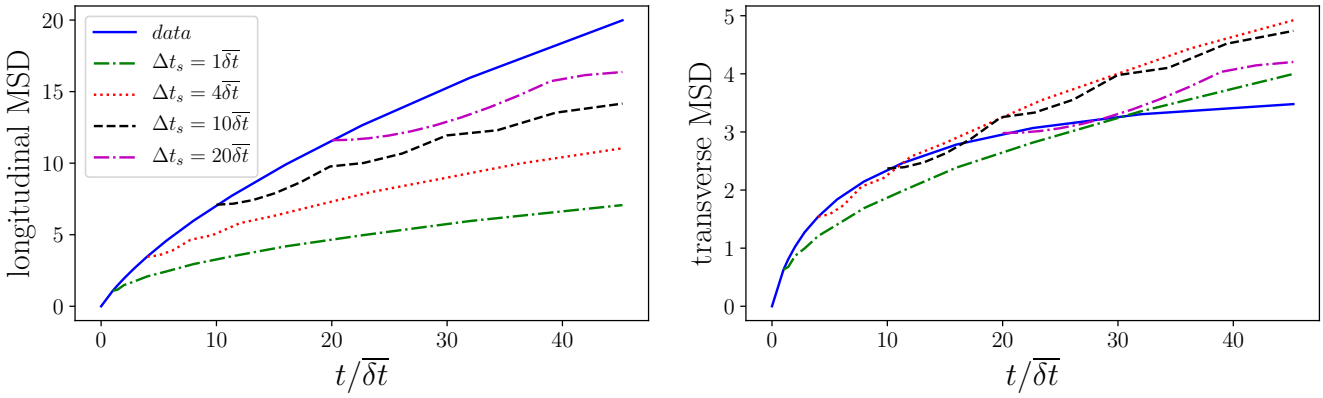

Figure 15: The evolution of the dimensionless second central moments of the plume for the exponential correlation structure compared with the moments predicted by independent sampling from $p(v, \theta)$.

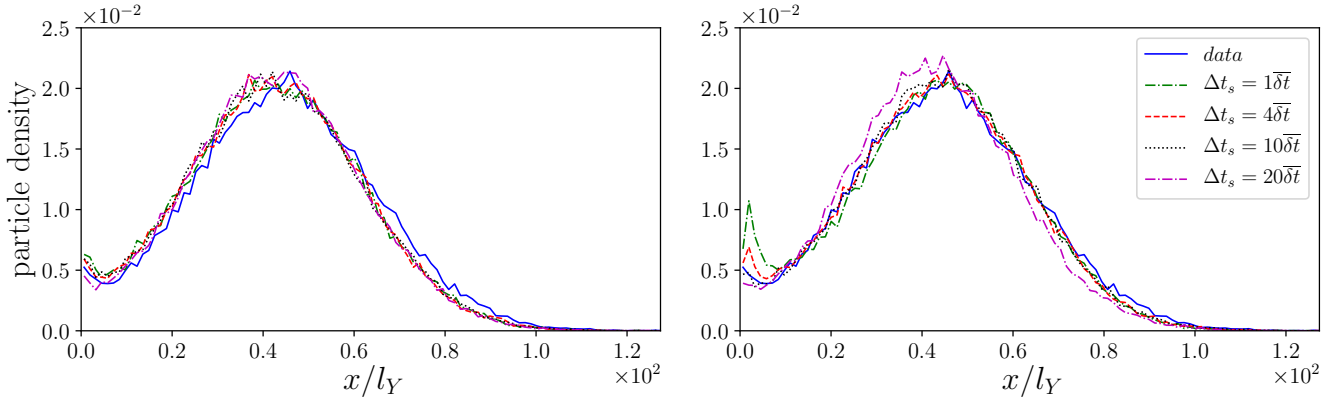

Figure 16: Comparison of the projected plume on the longitudinal direction for the exponential correlation structure at $t = 45\overline{\delta t}$; left: stencil method, right: DTMVP.

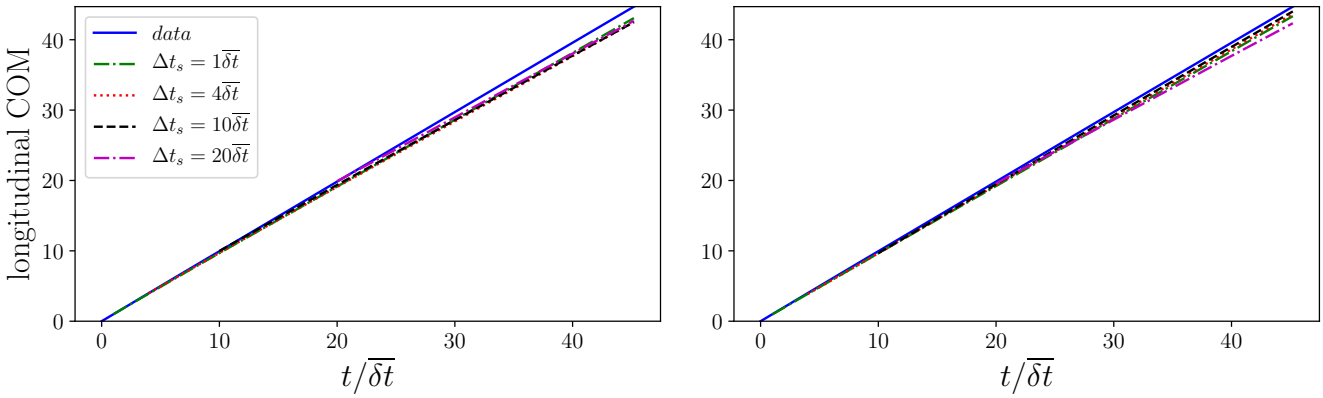

Figure 17: The evolution of the dimensionless longitudinal component of the plume center of mass for the exponential correlation structure; left: stencil method, right: DTMVP.

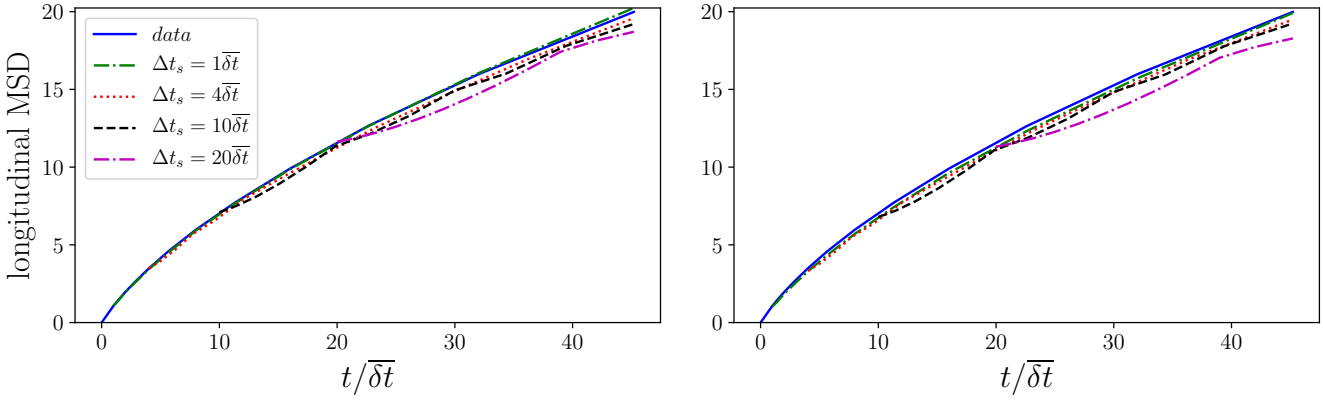

Figure 18: The evolution of the dimensionless second central moment of the plume in the longitudinal direction for the exponential correlation structure; left: stencil method, right: DTMVP.

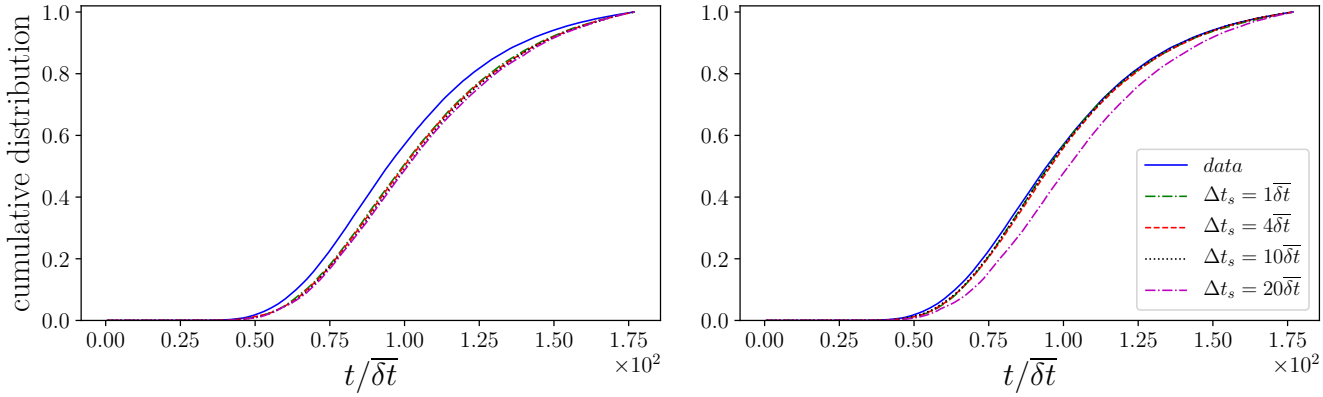

Figure 19: Comparison of the BT curve for the vertical plane $x = 0.75L$ for the exponential correlation structure; left: stencil method, right: DTMVP.

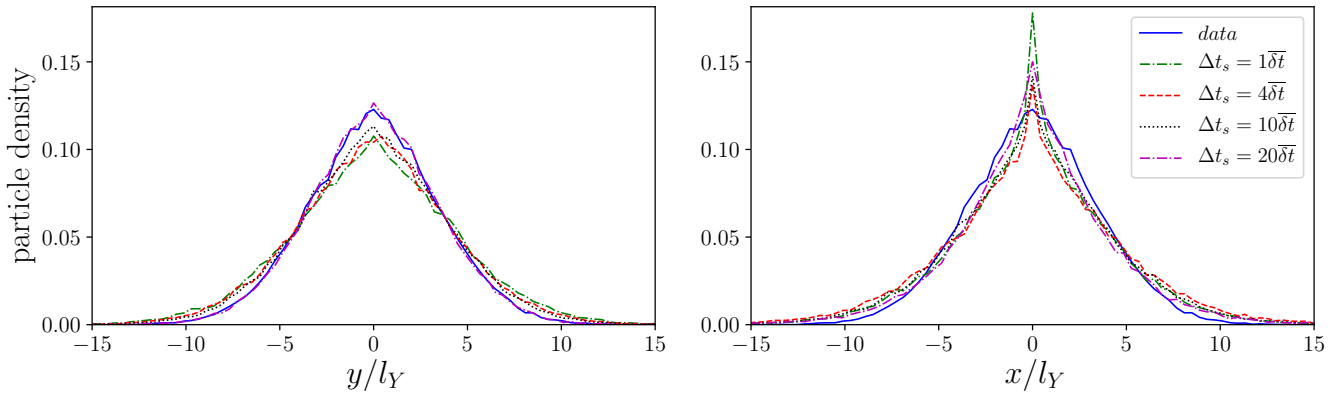

Figure 20: Comparison of the projected plume on the transverse direction for the exponential correlation structure at $t = 45\overline{\delta t}$; left: stencil method, right: DTMVP.

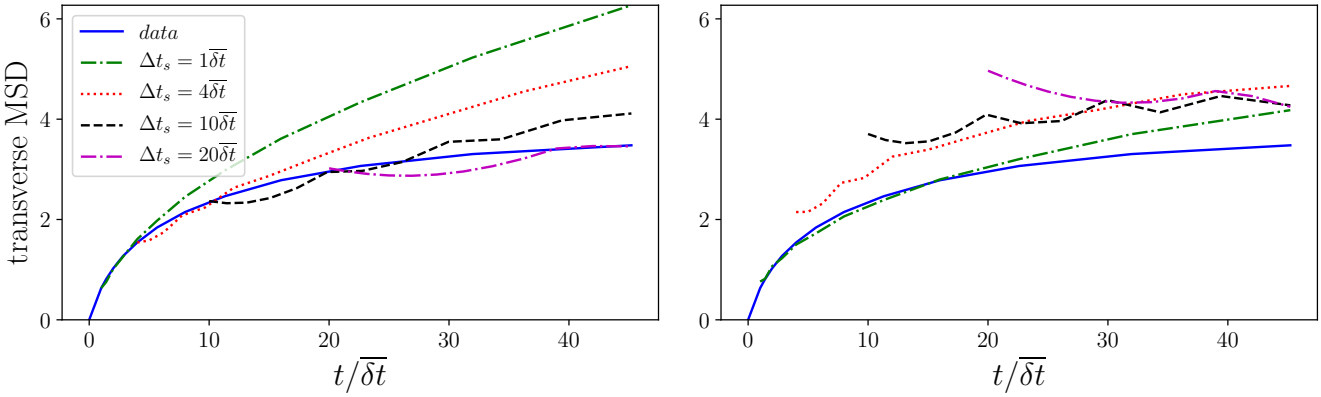

Figure 21: The evolution of the dimensionless second central moment of the plume in the transverse direction for the exponential correlation structure; left: stencil method, right: DTMVP.

References

1. Berkowitz B, Cortis A, Dentz M, Scher H. Modeling non-fickian transport in geological formations as a continuous time random walk. *Reviews of Geophysics* 2006;44(2).
2. Bouchaud JP, Georges A. Anomalous diffusion in disordered media: statistical mechanisms, models and physical applications. *Physics reports* 1990;195(4-5):127–293.
3. Edery Y, Guadagnini A, Scher H, Berkowitz B. Origins of anomalous transport in heterogeneous media: Structural and dynamic controls. *Water Resources Research* 2014;50(2):1490–505.
4. Nowak W, Rubin Y, Barros FP. A hypothesis-driven approach to optimize field campaigns. *Water Resources Research* 2012;48(6).
5. Moslehi M, de Barros FP. Uncertainty quantification of environmental performance metrics in heterogeneous aquifers with long-range correlations. *Journal of Contaminant Hydrology* 2017;196:21–9.
6. Ghorbanidehno H, Kokkinaki A, Li JY, Darve E, Kitanidis PK. Real-time data assimilation for large-scale systems: The spectral kalman filter. *Advances in Water Resources* 2015;86:260–72.
7. Fiori A, Zarlenga A, Gotovac H, Jankovic I, Volpi E, Cvetkovic V, Dagan G. Advective transport in heterogeneous aquifers: Are proxy models predictive? *Water resources research* 2015;51(12):9577–94.
8. Banton O, Delay F, Porel G. A new time domain random walk method for solute transport in 1–d heterogeneous media. *Ground Water* 1997;35(6):1008–13.
9. Bodin J, Porel G, Delay F. Simulation of solute transport in discrete fracture networks using the time domain random walk method. *Earth and Planetary Science Letters* 2003;208(3):297–304.
10. Graham W, McLaughlin D. Stochastic analysis of nonstationary subsurface solute transport: 1. unconditional moments. *Water Resources Research* 1989;25(2):215–32. URL: http://dx.doi.org/10.1029/WR025i002p00215. doi:doi: 10.1029/WR025i002p00215.
11. Le Borgne T, de Dreuzy JR, Davy P, Bour O. Characterization of the velocity field organization in heterogeneous media by conditional correlation. *Water resources research* 2007;43(2).
12. Le Borgne T, Dentz M, Carrera J. Lagrangian statistical model for transport in highly heterogeneous velocity fields. *Physical review letters* 2008;101(9):090601.
13. Le Borgne T, Dentz M, Carrera J. Spatial markov processes for modeling lagrangian particle dynamics in heterogeneous porous media. *Physical Review E* 2008;78(2):026308.
14. Kang PK, Dentz M, Le Borgne T, Juanes R. Spatial markov model of anomalous transport through random lattice networks. *Physical review letters* 2011;107(18):180602.
15. Kang PK, Dentz M, Le Borgne T, Juanes R. Anomalous transport on regular fracture networks: Impact of conductivity heterogeneity and mixing at fracture intersections. *Physical Review E* 2015;92(2):022148.
16. Kang PK, Le Borgne T, Dentz M, Bour O, Juanes R. Impact of velocity correlation and distribution on transport in fractured media: Field evidence and theoretical model. *Water Resources Research* 2015;51(2):940–59.
17. Delgoshaie AH, Jenny P, Tchelepi HA. Temporal markov processes for transport in porous media: random lattice networks. *Water Resources Research* 2018;54(5):3376–91.
18. Kang PK, De Anna P, Nunes JP, Bijeljic B, Blunt MJ, Juanes R. Pore-Scale intermittent velocity structure underpinning anomalous transport through 3-D porousmedia. *Geophysical Research Letters* 2014;41(17):6184–90. doi:doi: 10.1002/2014GL061475.
19. Kang PK, Dentz M, Le Borgne T, Lee S, Juanes R. Anomalous transport in disordered fracture networks: spatial markov model for dispersion with variable injection modes. *Advances in Water Resources* 2017;.
20. Meyer DW, Tchelepi HA. Particle-based transport model with markovian velocity processes for tracer dispersion in highly heterogeneous porous media. *Water Resources Research* 2010;46(11).
21. Meyer DW, Jenny P, Tchelepi HA. A joint velocity-concentration pdf method for tracer flow in heterogeneous porous media. *Water Resources Research* 2010;46(12).
22. Meyer DW, Saggini F. Testing the markov hypothesis in fluid flows. *Physical Review E* 2016;93(5):053103.
23. Meyer DW, Tchelepi HA, Jenny P. A fast simulation method for uncertainty quantification of subsurface flow and transport. *Water Resources Research* 2013;49(5):2359–79.
24. Meyer DW, Bijeljic B. Pore-scale dispersion: Bridging the gap between microscopic pore structure and the emerging macroscopic transport behavior. *Physical Review E* 2016;94(1):013107.
25. Attinger S, Dentz M, Kinzelbach W. Exact transverse macro dispersion coefficients for transport in heterogeneous porous media. *Stochastic Environmental Research and Risk Assessment* 2004;18(1):9–15. URL: http://dx.doi.org/10.1007/s00477-003-0160-6. doi:doi: 10.1007/s00477-003-0160-6.
26. Pardo-Iguzquiza E. The fourier integral method: an efficient spectral method for simulation of random fields. *Mathematical geology* 1993;25(2):177.
27. Bell WN, Olson LN, Schroder JB. PyAMG: Algebraic multigrid solvers in Python v3.0. 2015. URL: https://github.com/pyamg/pyamg; release 3.2.
28. Pollock DW. Semianalytical Computation of Path Lines for Finite-Difference Models. *Ground Water* 1988;26(6):743–50. URL: http://dx.doi.org/10.1111/j.1745-6584.1988.tb00425.x.
29. Delgoshaie AH. Repository including code and data for this work. To be released upon publication. 2018.

Appendix A. Supporting figures for Gaussian correlation structure

This appendix is provided to support the claim that the discrete temporal Markov velocity process (DTMVP) can be used to model transport in conductivity fields with a Gaussian correlation structure as well as exponential conductivity fields. The results of applying the DTMVP model to a conductivity field with a Gaussian correlation structure with a correlation length $l_Y = 8$ and variance of 4 are presented below.

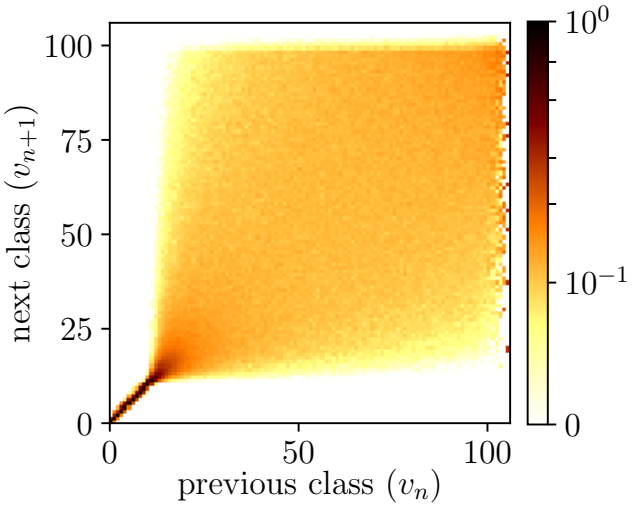

Figure A.1: $p_1^v(i|j)$ for the Gaussian correlation structure for $\Delta t_s = 10\overline{\delta t}$. Square root of the transition matrix is plotted for better contrast.

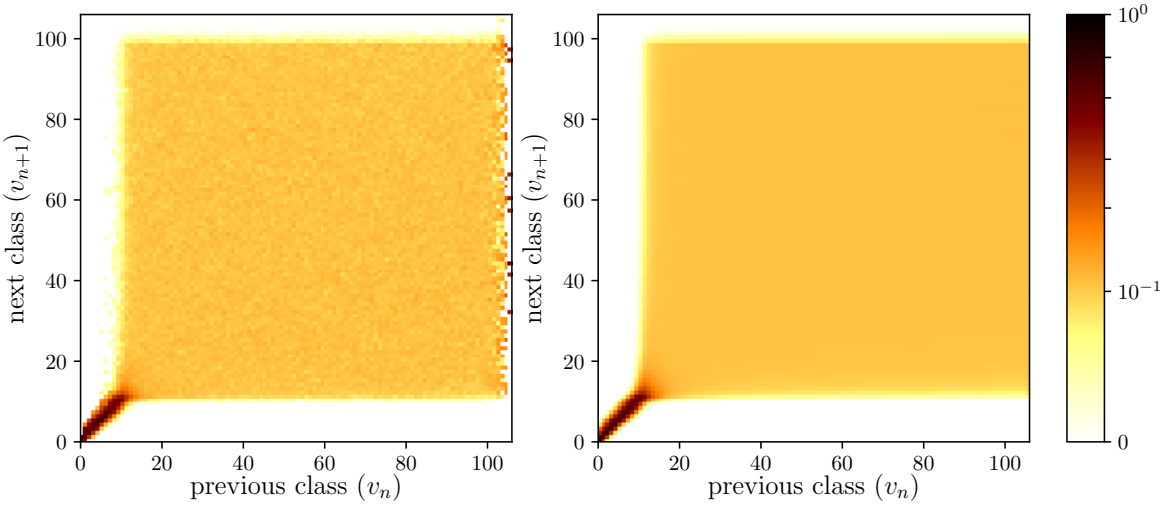

Figure A.2: Comparison of $p_5^v(i,j)$ (left) and $p_1^v(i,j)^5$ (right) for the Gaussian correlation structure for $\Delta t_s = 10\overline{\delta t}$. Square root of the transition matrices are plotted for better contrast.

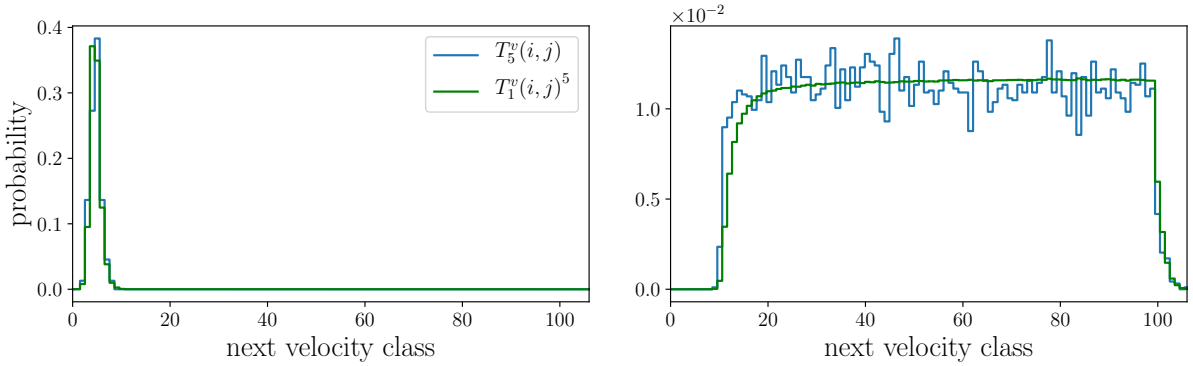

Figure A.3: Column-wise comparison of $p_5^v(i,j)$ and $p_1^v(i,j)^5$ for the Gaussian correlation structure for $\Delta t_s = 10\overline{\delta t}$. Left: initial class $j = 4$; right: initial class $j = 62$.

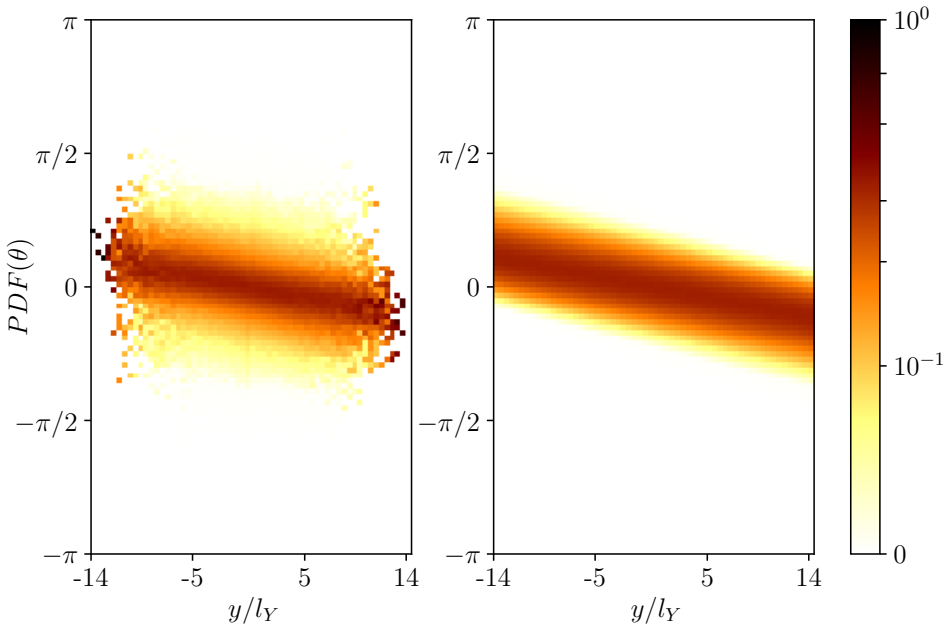

Figure A.4: $P(\theta|y)$ for the Gaussian correlation structure with $\Delta t_s = 10\overline{\delta t}$. Left: empirical distribution from MC simulations; right: modeled histogram using the extrapolated moments of Pearson3 distribution.

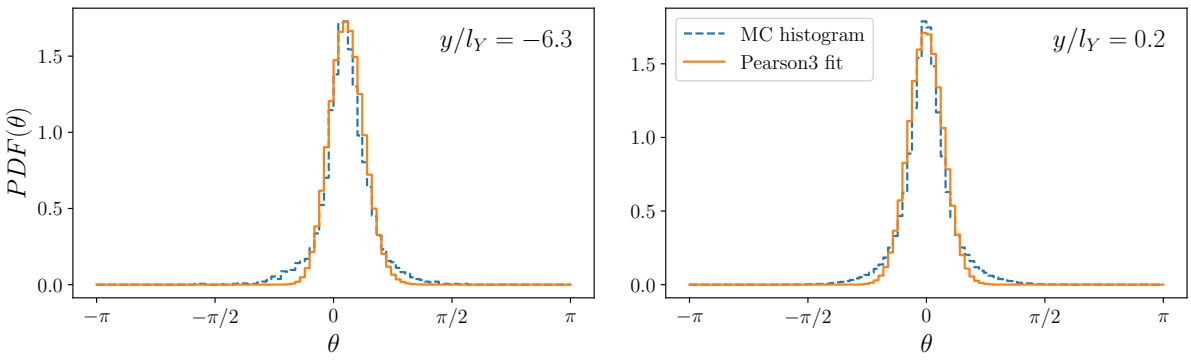

Figure A.5: Comparison of $P(\theta|\overline{y})$ for two different values of $\overline{y}$ for the Gaussian correlation structure for $\Delta t_s = 10\overline{\delta t}$.

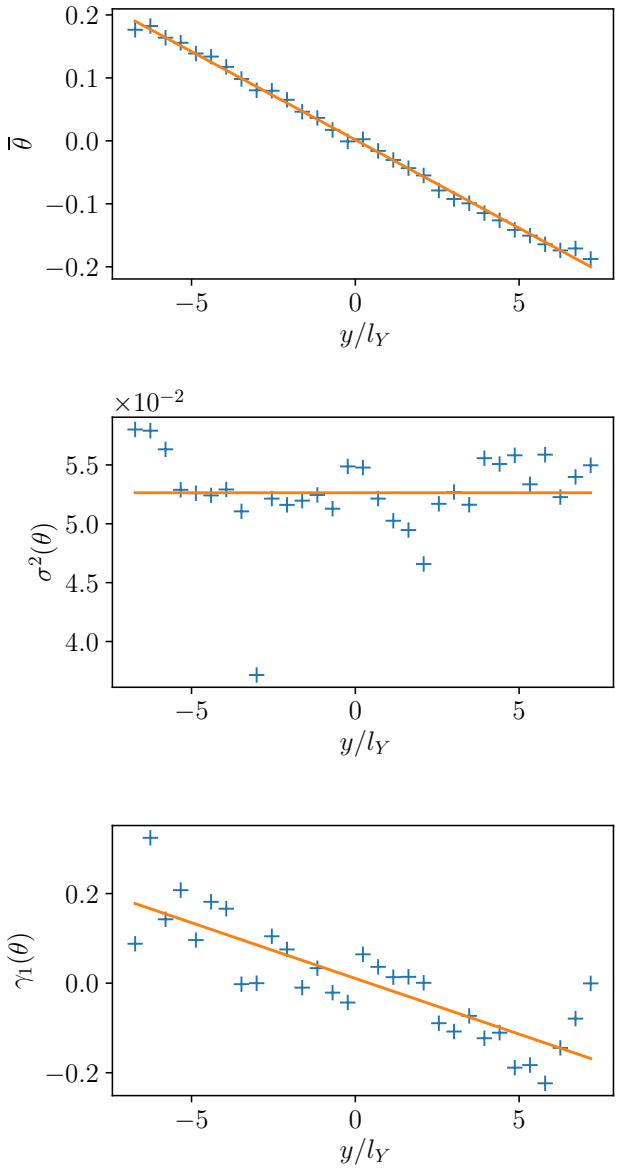

Figure A.6: First three moments of $P(\theta|\overline{y})$ as a function of $\overline{y}$, for the Gaussian correlation structure with $\Delta t_s = 10\overline{\delta t}$.

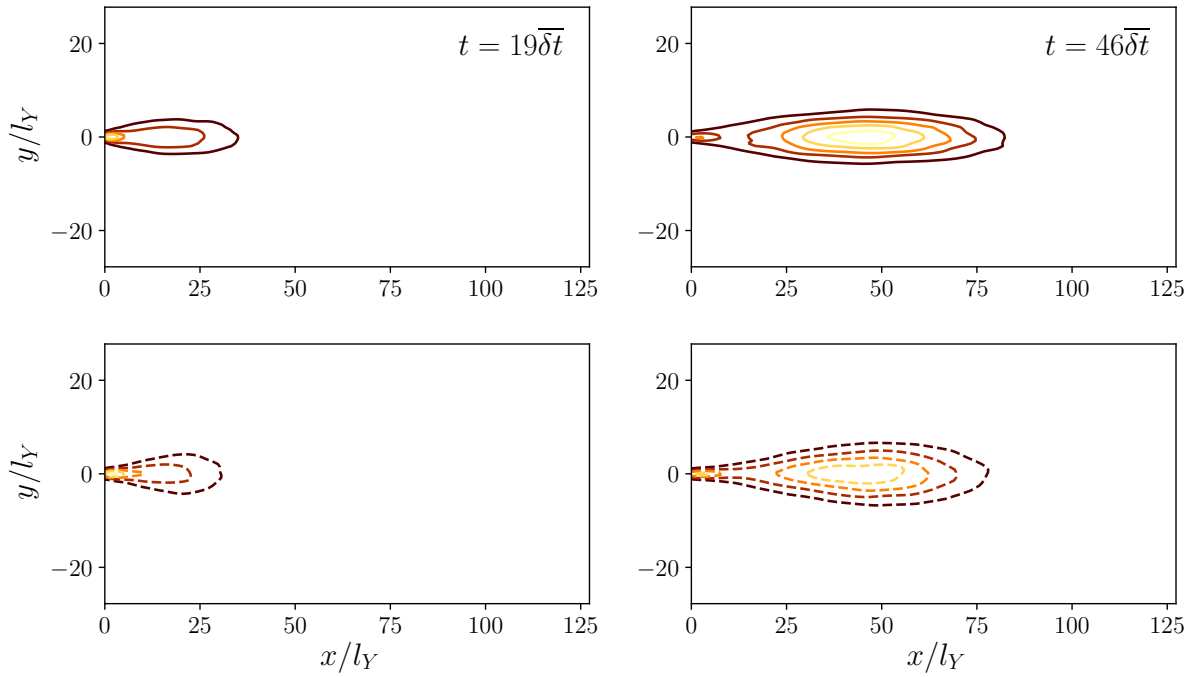

Figure A.7: Comparison of the predicted plume (solid lines) versus the MC data (dashed lines) for two different times for the same contour levels for the Gaussian correlation structure.

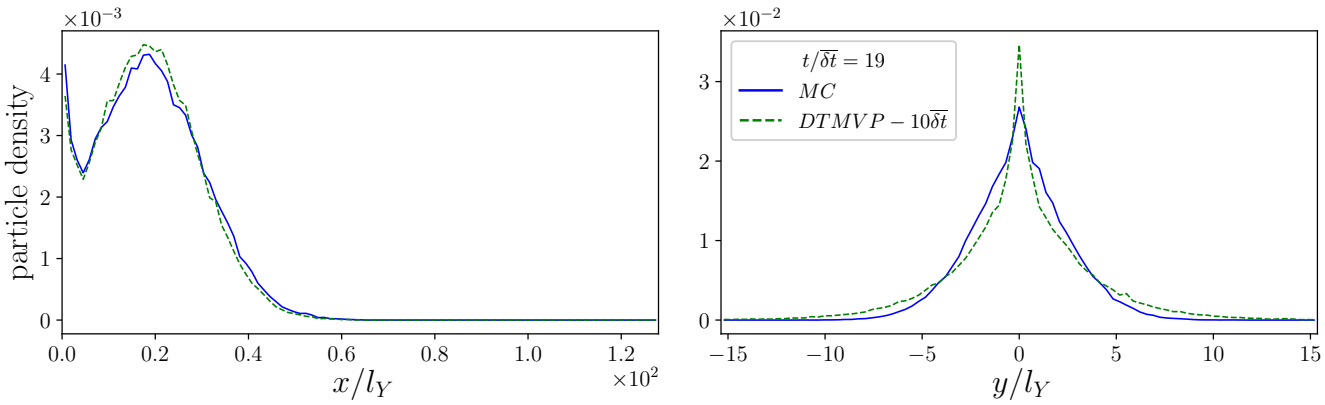

Figure A.8: Comparison of the predicted plume versus the MC data for $t = 19\overline{\delta t}$ for the Gaussian correlation structure.

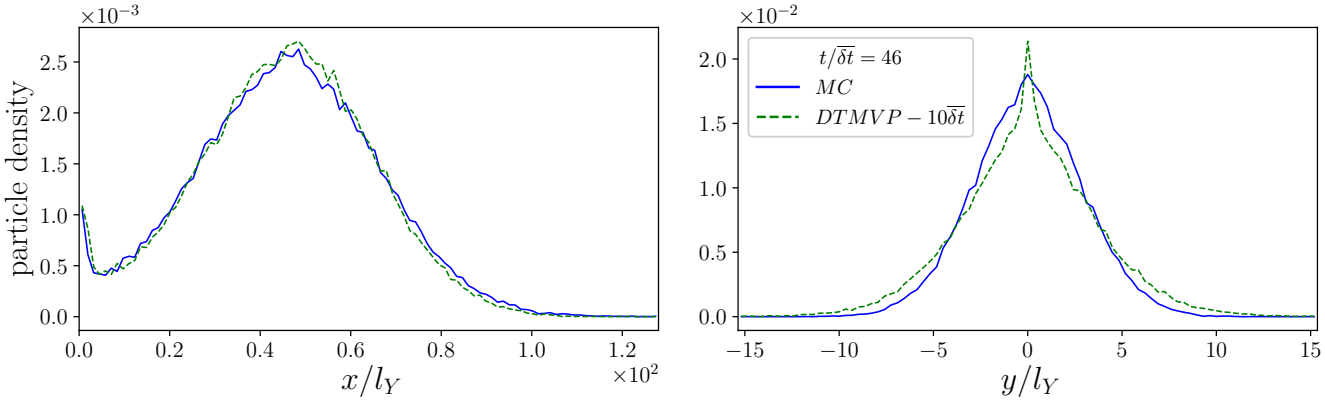

Figure A.9: Comparison of the predicted plume versus the MC data for $t = 46\overline{\delta t}$ for the Gaussian correlation structure.

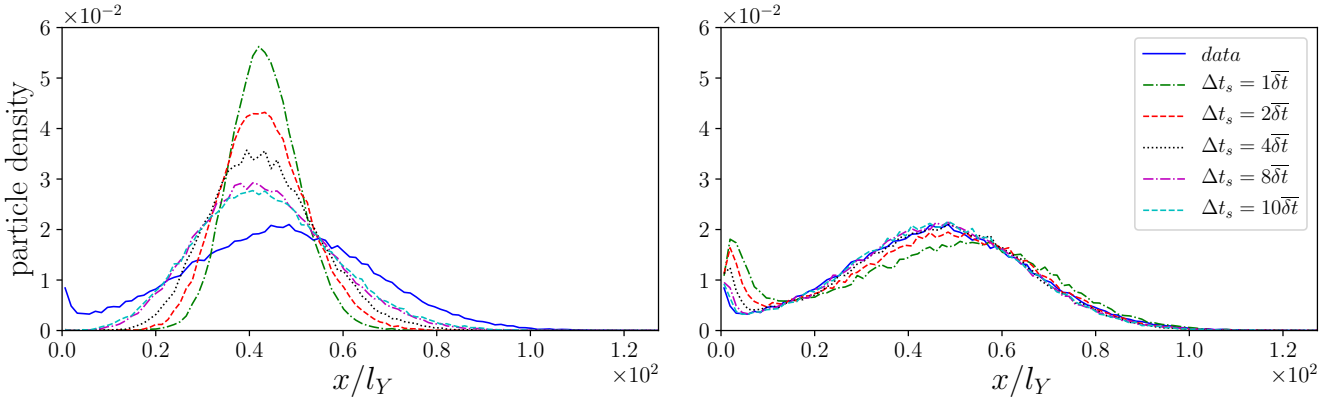

Figure A.10: Comparison of the predicted plumes from the independent model (left) and DTMVP (right) at $t = 46\overline{\delta t}$ for different time steps for the Gaussian correlation structure.

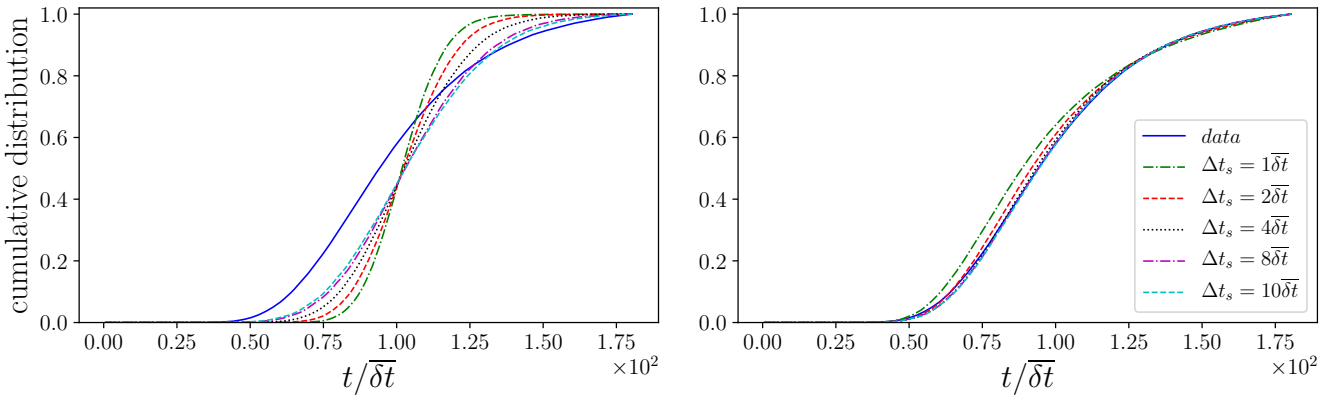

Figure A.11: Comparison of the predicted BT curves from the independent model (left) and DTMVP (right) at $x = 0.75L$ for different time steps for the Gaussian correlation structure.

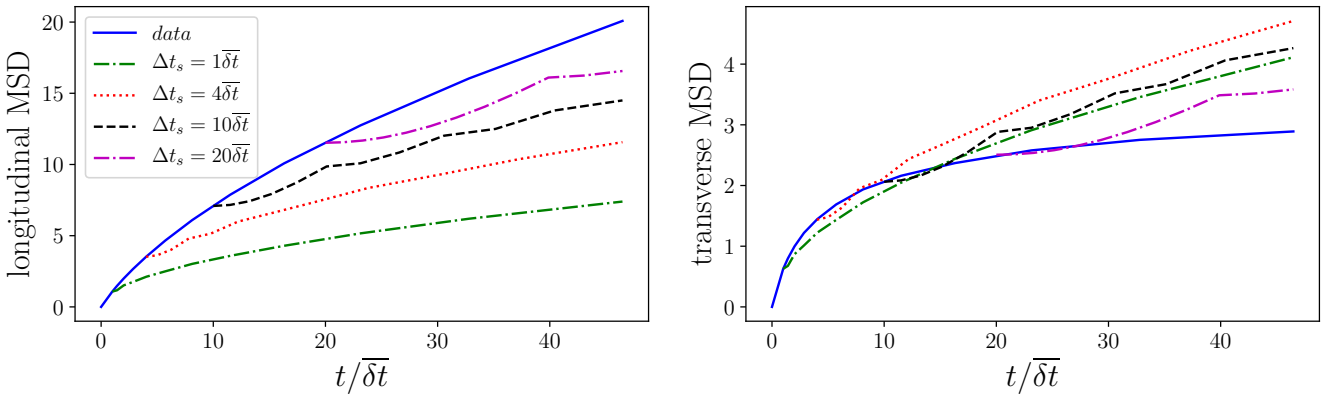

Figure A.12: The evolution of the second central moments of the plume for the Gaussian correlation structure compared with the moments predicted by independent sampling from $p(v, \theta)$.

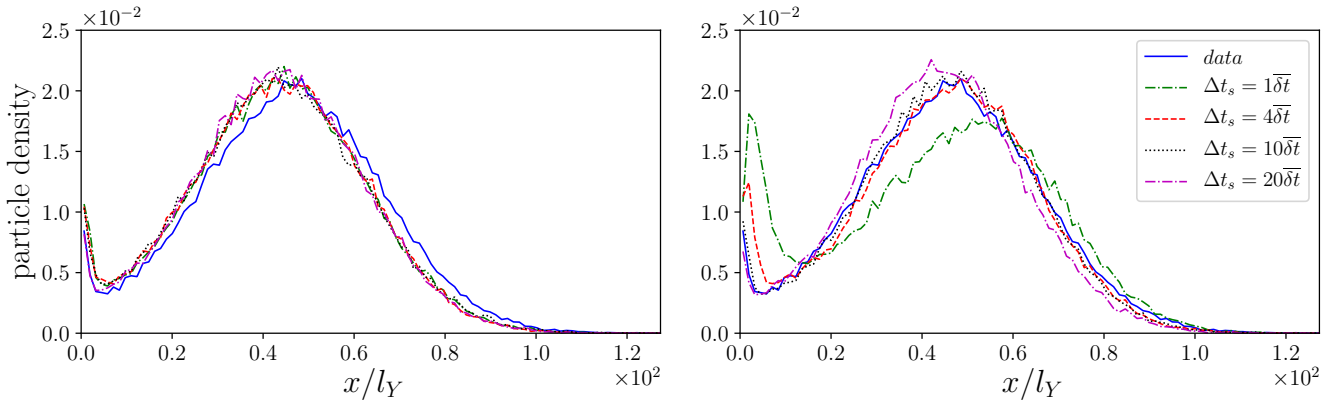

Figure A.13: Comparison of the projected plume on the longitudinal direction for the Gaussian correlation structure at $t = 46\overline{\delta t}$; left: stencil method, right: DTMVP.

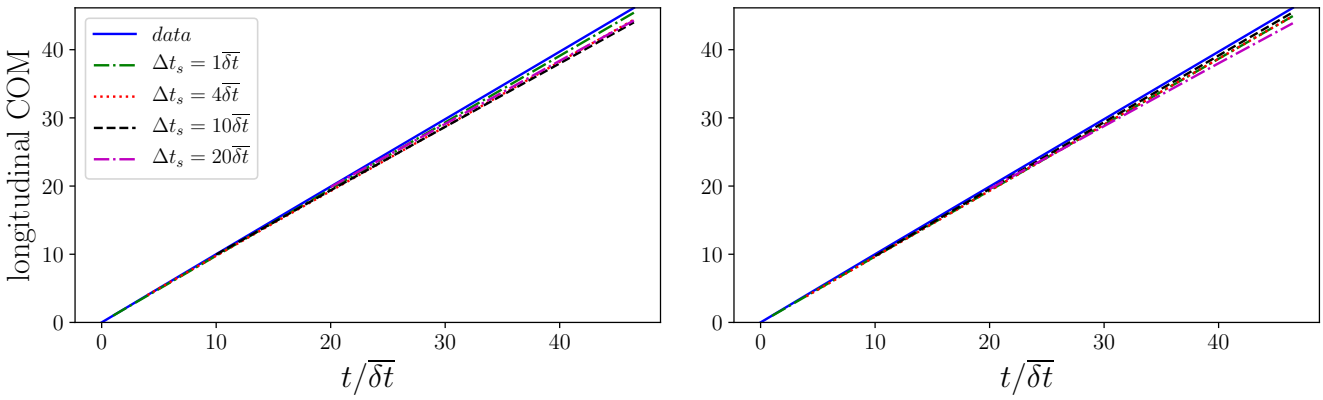

Figure A.14: The evolution of the dimensionless longitudinal component of the plume center of mass for the Gaussian correlation structure; left: stencil method, right: DTMVP.

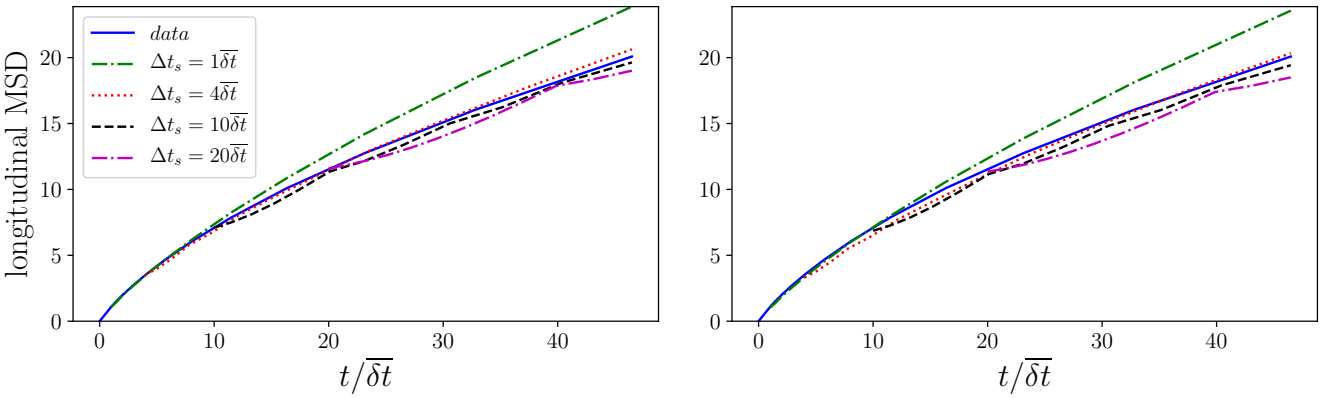

Figure A.15: The evolution of the dimensionless second central moment of the plume in the longitudinal direction for the Gaussian correlation structure; left: stencil method, right: DTMVP.

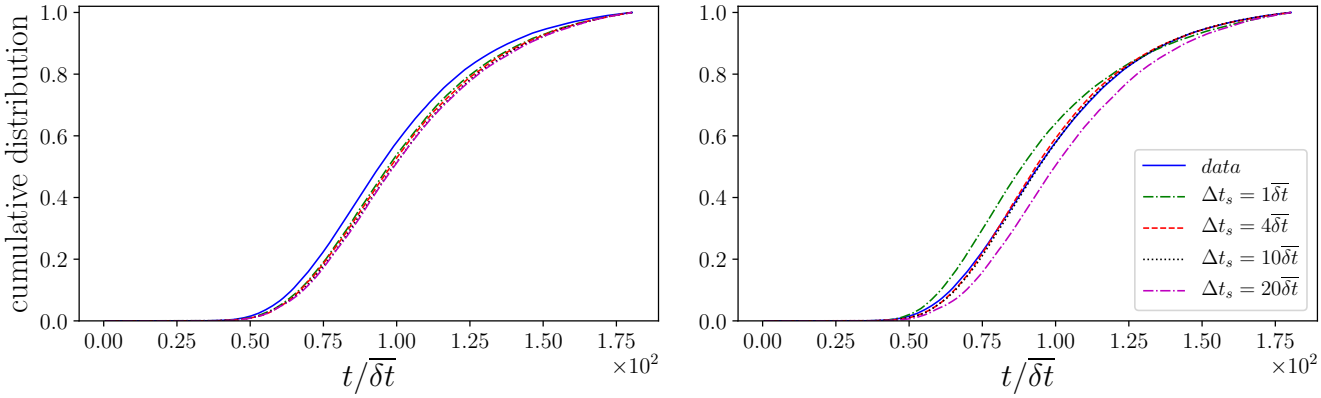

Figure A.16: Comparison of the BT curve for the vertical plane $x = 0.75L$ for the Gaussian correlation structure; left: stencil method, right: DTMVP.

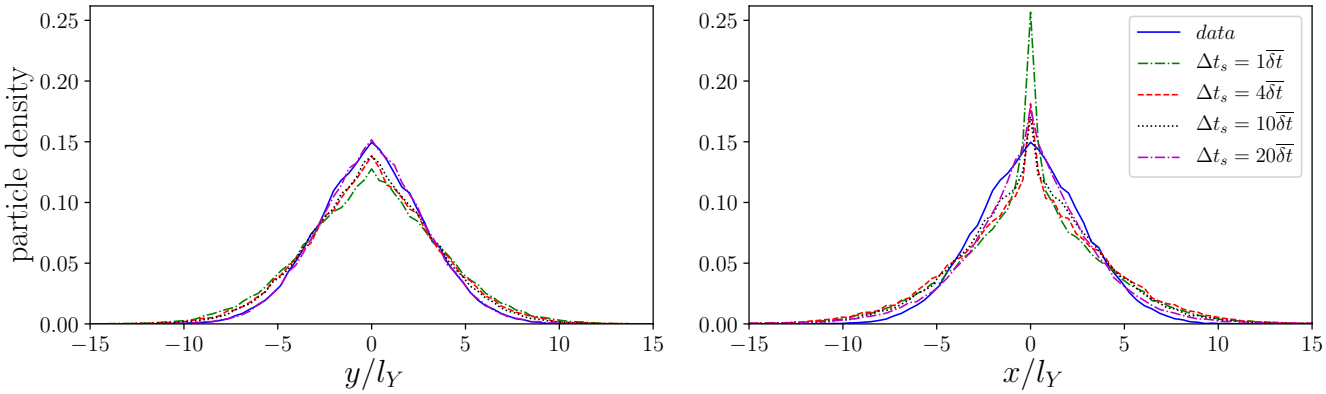

Figure A.17: Comparison of the projected plume on the transverse direction for the Gaussian correlation structure at $t = 46\overline{\delta t}$; left: stencil method, right: DTMVP.

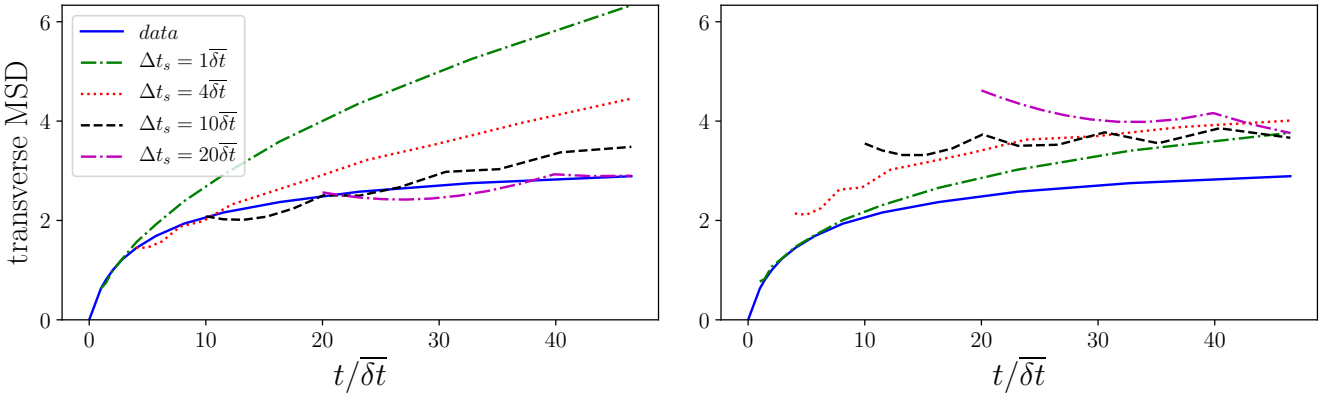

Figure A.18: The evolution of the dimensionless second central moment of the plume in the transverse direction for the Gaussian correlation structure; left: stencil method, right: DTMVP.